Supplementary Table 1: Bacterial strains and plasmids

***E.coli* strains**	**Relevant genotype**	**Ref.**
BW25113	Wild type (*pir-)*	Baba *et al* (2006)
BW25141	Wild type (*pir+)*	Datsenko and Wanner (2000)
Keio:cydb	BW25113 Δ*cydb::frt-kan-frt*	Baba *et al* (2006)
YTL01	BW25113 *cydB-gfpgcn4*	This study
Plasmids		
ASKA cydb-gfp	pCA24N::cydB-gfpgcn4	Kitagawa *et al* (2005)
pDS132	R6K*ori* RP4*mob cat sacB*	Phillippe *et al* (2004)
pYTL01	*pDS132 cydb-gfpgcn4*	This study

Supplementary Table 2: PCR primers used in the construction of plasmid pYTL01 (sequences 5'-3')

P1	TCGATTATGAAGTATTGCG
P2	CATTTTTAGCTCCTTACTTATTTGTATAGTTCATCC
P3	GGATGAACTATACAAATAAGTAAGGAGCTAAAAATG
P4	GCATATACTGCAGAAACGCTGCTACTATACG

Supplementary Methods 1

Fluorescence microscopy. We used a custom-made inverted fluorescence microscope (Leake *et al*, 2006; Lo *et al*, 2006; Lo *et al*, 2007) with x100 Plan Fluor 1.45 NA oil-immersion objective (Nikon UK Ltd., UK) and an *xyz* nanopositioning stage (E-503.00, Physik Instrumente, Germany). Laser excitation was with a TEM00 plane-polarized continuous-wave 473 nm laser (Oxxius, Laser2000 UK Ltd, Ringstead, UK), circularized for polarization, filtered (laser-line, 473 nm), expanded x3 and focussed onto the back-focal-plane of the objective lens via a dichroic mirror (505 nm long-pass). Controlled movement of the focus equated to rotation of the emergent angle from the objective permitting switching between epifluorescence and TIRF (measured 1/e evanescent field depth 97 ± 11 nm). The field width was ~30 μm and intensity ~140 W cm^{-2} (~3.9 kW cm^{-2} for *in vitro* measurements on surface-immobilized GFP molecules (Leake *et al.,* 2006). A separately-shuttered excitation path allowed some of the laser light to be focussed in the sample plane to a width ~1.0 μm, intensity ~50 kW cm^{-2}. For FRAP experiments this second path was used to bleach a cell pole for typically ~0.5 s, illumination from the first path was used to monitor fluorescence changes continuously. The focal plane was at either 100 nm (TIRF) or mid-cell height of ~0.5 μm (epifluorescence) from the surface of the microscope coverslip. Emission was passed through the dichroic mirror, a band-pass filter (530 nm) and a notch rejection filter (473 nm), and imaged at magnification ~50 nm per pixel in frame-transfer mode at 25 Hz onto a 128x128-pixel, cooled, back-thinned electron-multiplying charge-coupled-device camera (iXon DV860-BI, Andor Technology, UK).

References

Leake, MC, Chandler JH, Wadhams GH, Fan B, Berry RM, Armitage JA (2006) Stoichiometry and turnover in single, functioning membrane protein complexes. *Nature* **433**: 355-358.

Lo C-J, Leake MC, Berry RM (2006) Fluorescence measurement of intracellular sodium concentration in single *Escherichia coli* cells. *Biophys J* **90**: 357-365.

Lo C-J, Leake MC, Pilizota T, Berry RM (2007) Nonequivalence of membrane voltage and ion-gradient as driving forces for the bacterial flagellar motor at low load. *Biophys J* **93**: 294-302.

Supplementary Methods 2

Detection of fluorescent spots in cells. Custom-written pattern recognition software (LabVIEW 8.1, National Instruments, Austin, TX) was applied to locate cell borders from the brightfield images. This was used to create an image mask for fluorescence analyses, padding each cell perimeter by a point spread function. Fluorescent spots were auto-detected using custom-written code to locate circular intensity distributions of width 100- 350 nm (Danielsson distance map algorithm). A circular region of interest (ROI) was then created around each spot of radius 300 nm. Intensity in each was modelled as a radial Gaussian plus a uniform baseline due to a combination of cell autofluorescence, non-cell background and diffusing CydB-GFP not bound in spots:

1. We used a circular mask for the contribution of the CydB-GFP spot , diameter 5 pixels to the ROI, centred on the current intensity centroid.

2. We multiplied intensities within the mask by a 2-dimensional Gaussian mask. fixed half-width 150 nm, and generated a new estimate for the centroid (Thompson *et al*, 2002; Leake *et al*, 2006).

3. We iterated steps 1 and 2 either 10 times or until the mask started clipping the side of the initial ROI, resulting in an ultimate centroid precision of ~4 nm depending on spot brightness. A Gaussian fit was then performed on the spot intensity component optimising amplitude and width.

4. We defined the background intensity as the mean intensity within the ROI but outside the circular mask. We defined the spot intensity as the sum of all intensities within the circular mask after subtraction of the background from each individual pixel value.

5. We defined instrument background (non-cellular intensity) as the mean intensity in a circular ROI, diameter 8 pixels, containing no cells.

Steps 1-5 were performed separately on each image frame.

6. Cell autofluorescence was defined as the mean intensity minus the instrument background from circular ROIs, diameter 8 pixels located in the cylindrical region at the periphery of the cell (i.e. centred over a segment of cell membrane), from different cells of the parental strain not containing GFP.

7. The diffusive membrane intensity component of background for each image was defined as the total background minus the instrument component (step 5) and the cell autofluorescence component (step 6).

To characterise GFP photobleaching a mean intensity versus time trace was calculated and fitted by a single exponential decay function. Intensity data from the parental cell strain was treated similarly to characterize cell autofluorescence

Defining tracks of spots. The properties of each spot were compared to those detected in the previous image in a series (Leake *et al.*, 2008). If the nearest detected spot to a previous position met the criteria below it was classed as the same spot:

1. The previous spot position is within 250 nm of the new position.
2. Spot intensity must change by less than 50%.
3. The width must change by less than 50%.

If two separate spot tracks are within 250 nm of each other both are terminated. Only tracks consisting of at least three consecutive image frames are used for subsequent analysis.

Coordinate transformation. Spot positions were recorded in the co-ordinate system of the camera; however spot movements were consistent with diffusion over a cell membrane surface. Therefore we transformed into the surface co-ordinate system appropriate for each individual cell. A spot was first assigned into one of three zones based on the brightfield image mask data of its corresponding cell: a central cylindrical region or one of two hemispherical caps. The spot *xy* co-ordinates were transformed into either cylindrical or spherical polars as appropriate, $x'y'$. A track was partitioned into two separate tracks if it crossed the focal plane, though continuity was permitted if it crossed from a cylindrical into a hemispherical region (or vice-versa).

Estimation of average number of spots per cell. The number of CydB-GFP tracks detected after the initial focused laser bleach during subsequent continuous epifluorescence excitation at 25 Hz frame-rate was estimated for each cell and corrected for photobleaching during normal epifluorescence illumination, indicating a mean of 4.1 ± 1.1 (±s.d., using 54 cells) tracks per cell per frame. The depth-of-focus for typical GFP spectral emissions was estimated to be 360 ± 20 nm, consistent with theoretical predications. Modelling the cell as a cylinder of length 2 μm, diameter 1 μm, capped at either end with 1 μm diameter hemispheres (Leake *et al*, 2006) indicates that the field of focus encapsulates ~10 % of the membrane surface, indicating a mean total number of photoactive spots per cell after the focused laser bleach of 41 ± 11, which compares well to the total number of tracks detected (2062) from a population of 54 cells (i.e. ~38 tracks per cell). However, the ratio of the total cellular pixel intensity (minus autofluorescence and instrumental background) just after the focused laser bleach to just before we measure to be 18 ± 4 %. This indicates the total number of spots per cell is 230 ± 80.

References

Leake MC, Chandler JH, Wadhams GH, Fan B, Berry RM, Armitage JA (2006) Stoichiometry and turnover in single, functioning membrane protein complexes. *Nature* **433**: 355-358.

Leake MC, Greene NP, Godun RM, Granjon T, Buchanan G, Chen S, Berry RM, Palmer T, Berks B.C. (2008) Variable stoichiometry of the TatA component of the twin-arginine protein transport system observed by *in vivo* single-molecule imaging. *Proc Natl Acad Sci U S A.* In Press.

Thompson RE, Larson DR, Webb WW (2002) Precise nanometer localization analysis for individual fluorescent probes. *Biophys J* **82**: 2775-2783.

Supplementary Methods 3

Estimation of CydB-GFP number in tracked complexes.

Estimation of CydB-GFP stoichiometry in spots utilised a method based on the step-wise photobleaching of GFP (Leake *et al*, 2006). We calculated the pairwise differences for all intensity traces *I(t)* recorded for each individual cell:

$\Delta I_{ij} = I(t_i)-I(t_j)$

for all data pairs for which the time $t_i > t_j$. The pairwise differences for all tracks recorded for every separate cell were then combined. The distribution of these combined differences (pairwise difference distribution function) was calculated using 3,000 bins and normalised by the total number of differences, $n(n - 1)/2$, where n is the number of data points in each trace (Kuo *et al*, 1991). We then calculated the power spectrum from each pairwise displacement histogram. Peak detection was automated using commercial code (LabView 8.1, National Instruments, Austin, TX) with the unitary step peak taken as that detected at the highest spatial frequency in each trace (Svoboda *et al*, 1993). A peak detection threshold was taken as four standard deviations above the high spatial frequency noise floor (defined as the standard deviation of the power spectrum signal between S_{fmax} and S_{fmax} /2, where S_{fmax} is the maximum spatial frequency for the power spectrum) equivalent to a probability confidence level of $P<0.001$. The corresponding value of spatial frequency was inverted to give the characteristic "unitary step size" I_{GFP} in terms of intensity counts, typically ~450 counts. This value was broadly consistent with integer multiples of the individual steps in the photobleach trace measured using Chung-Kennedy filtration and edge-detection algorithms (Leake *et al*., 2003; Leake *et al.* 2004), but simulations indicated that the Fourier analysis approach was more accurate for estimating I_{GFP}.

Each individual intensity trace for both membrane and complex components was then fit with a single exponential decay function $I(t)=I_0\exp(-t/t_0)$, constraining t_0 to the mean GFP bleach time constant of 45 ± 6 s as measured previously (Supplementary Methods 2). The number of CydB-GFP molecules associated with each diffusing complex was then estimated as the initial intensity of the complex component I^C_0 prior to any photobleaching divided by I_{GFP}. Similarly, the total pixel count for the membrane CydB-GFP component was calculated as follows:

1. We took the mean of the initial total intensity of the membrane component (after subtracting the autofluorescence contribution and instrumental background) associated with each detected spot. We then normalized it by the number of equivalent cubic pixels in the corresponding voxel region of interest. The voxel region of interest was approximated as the number of complete pixel squares between the boundary of each detected spot and the 8 pixel diameter circular region around each spot (typically 25-30 pixels^2) on the 2D image plane multiplied by the depth of field (~370 nm) of ~7.4 pixels, giving 185-222 pixels^3).

2. We then multiplied this normalized intensity by the total number of squared pixels associated with the cell-surface area estimated from the brightfield image of the cell, which had a mean consistent with previously measured values of *Escherichia coli* of 3700 ± 500 pixels^2 (Leake *et al*, 2006).

3. We divided this estimate for total intensity associated with the membrane by I_{GFP} to generate an estimate for the total number of photoactive GFP molecules in the membrane.

4. We did this for each cell, and then calculated the mean value corresponding to this distribution. This indicated the total CydB-GFP content not associated with distinct spots is 2,300 ± 830 CydB-GFP per cell.

5. The total average CydB-GFP component associated with spots was approximated by multiplying the mean value of CydB-GFP stoichiometry per spot (76 ± 33 CydB-GFP molecules, Fig. 4) by the mean number of spots observed cell per frame corrected for photobleaching (230 ± 80 spots per cell). This indicated 17,500 ± 9,900 CydB-GFP molecules per cell.

6. To estimate the total membrane content of CydB-GFP in each we added this value to the estimate from (4) above. This suggested a total content (i.e. foci plus non-foci) of 19,800 ± 9,900 CydB-GFP molecules per cell.

References

Kuo SC, Gelles J, Steuer E, Sheetz MP (1991) A model for kinesin movement from nanometer-level movements of kinesin and cytoplasmic dynein and force measurements. *J Cell Sci* **14**: 135-138.

Leake MC, Wilson D, Bullard B and Simmons RM (2003) The elasticity of single kettin molecules using a two-bead laser-tweezers assay. *FEBS Lett.* **535**: 55-60.

Leake MC, Wilson D, Gautel M and Simmons RM (2004) The elasticity of single titin molecules using a two-bead optical tweezers assay. *Biophys. J.* **87**: 1112-1135.

Leake MC, Chandler JH, Wadhams GH, Fan B, Berry RM, Armitage JA (2006) Stoichiometry and turnover in single, functioning membrane protein complexes. *Nature* **433**: 355-358.

Svoboda K, Schmidt CF, Schnapp BJ, Block SM (1993) Direct observation of kinesin stepping by optical trapping interferometry. *Nature* **365**: 721-727.

Supplementary Methods 4

Calculating diffusion coefficients

After curvilinear coordinate transformation the mean-squared displacement (*MSD*) for a track of N consecutive image frames at a time intervals $\tau=n\Delta t$ is (Gross and Webb, 1988):

$$MSD(\tau) = MSD(n\Delta t) = \frac{1}{N-1-n}\sum_{i=1}^{N-1-n}\left\{\left[x'(i\Delta t + n\Delta t) - x'(i\Delta t)\right]^2 + \left[y'(i\Delta t + n\Delta t) - y'(i\Delta t)\right]^2\right\}$$

To distinguish normal and restricted diffusion we used the relative deviation parameter (Kusumi *et al*, 1993) $RD(n, N)=MSD(n, N)/4\tau D_{2\text{-}4}$ for which $D_{2\text{-}4}$ is a measure of the diffusion at low τ values based only on a straight-line fit of *MSD* versus τ (slope $4D_{2\text{-}4}$) such that $2\Delta t \leq \tau \leq 4\Delta t$, Δt is the image frame time (40 ms). Normal Brownian diffusion satisfies $MSD(\tau)=4D\tau$, D is the effective two-dimensional diffusion coefficient, implying $RD=1$. If diffusion is restricted lower *RD* values are observed. To find a threshold for *RD* to distinguish between these modes we used a Student *t*-test to *MSD* data from high ($N\Delta t/2<\tau\leq N\Delta t$) and low ($\Delta t\leq\tau\leq N\Delta t/2$) time interval regimes on each track such that if the mean *MSD* was significantly greater (P>0.5) for high time compared to low then the mode was categorized as normal, otherwise as restricted. The threshold, RD_{thresh}, of minimum (*RD*) was defined as when P(putatively restricted, minimum (*RD*)<RD_{thresh})=P(putatively normal, minimum (*RD*)≥RD_{thresh}). The data indicates RD_{thresh}=0.30 and P(putatively restricted, minimum (*RD*)<RD_{thresh})=0.64.

Analysis of restricted diffusion. Restricted diffusion was modelled (Kusumi *et al*, 1993) by:

$$MSD = L^2\left(\frac{1}{6} - \frac{16}{\pi^4}\sum_{k=1(odd)}^{\infty}\frac{1}{k^4}\exp\left\{-\left(\frac{k\pi}{L}\right)^2 D_\mu\tau\right\}\right) \approx \frac{L^2}{6}\left(1-\exp\left\{-\frac{\tau}{\tau_\mu}\right\}\right),$$

D_μ is the microscopic diffusion coefficient, L effective restricting compartment diameter and τ_μ a measure of the time interval over which diffusion within the compartment is normal. Using the average *MSD* trace generated from all restricted diffusion indicates L=160 ± 30 nm (±s.d).

References

Gross DJ, Webb WW (1988) Cell surface clustering and mobility of the liganded LDL receptor measured by digital video fluorescence microscopy. In *Spectroscopic Membrane Probes II*, Loew LM (ed). pp 19-45, Boca Raton, FL: CRC Press.

Kusumi A, Sako Y, Yamamoto M (1993) Confined lateral diffusion of membrane receptors as studied by single particle tracking (nanovid microscopy). effects of calcium-induced differentiation in cultured epithelial cells. *Biophys J* **65**: 2021-2040.

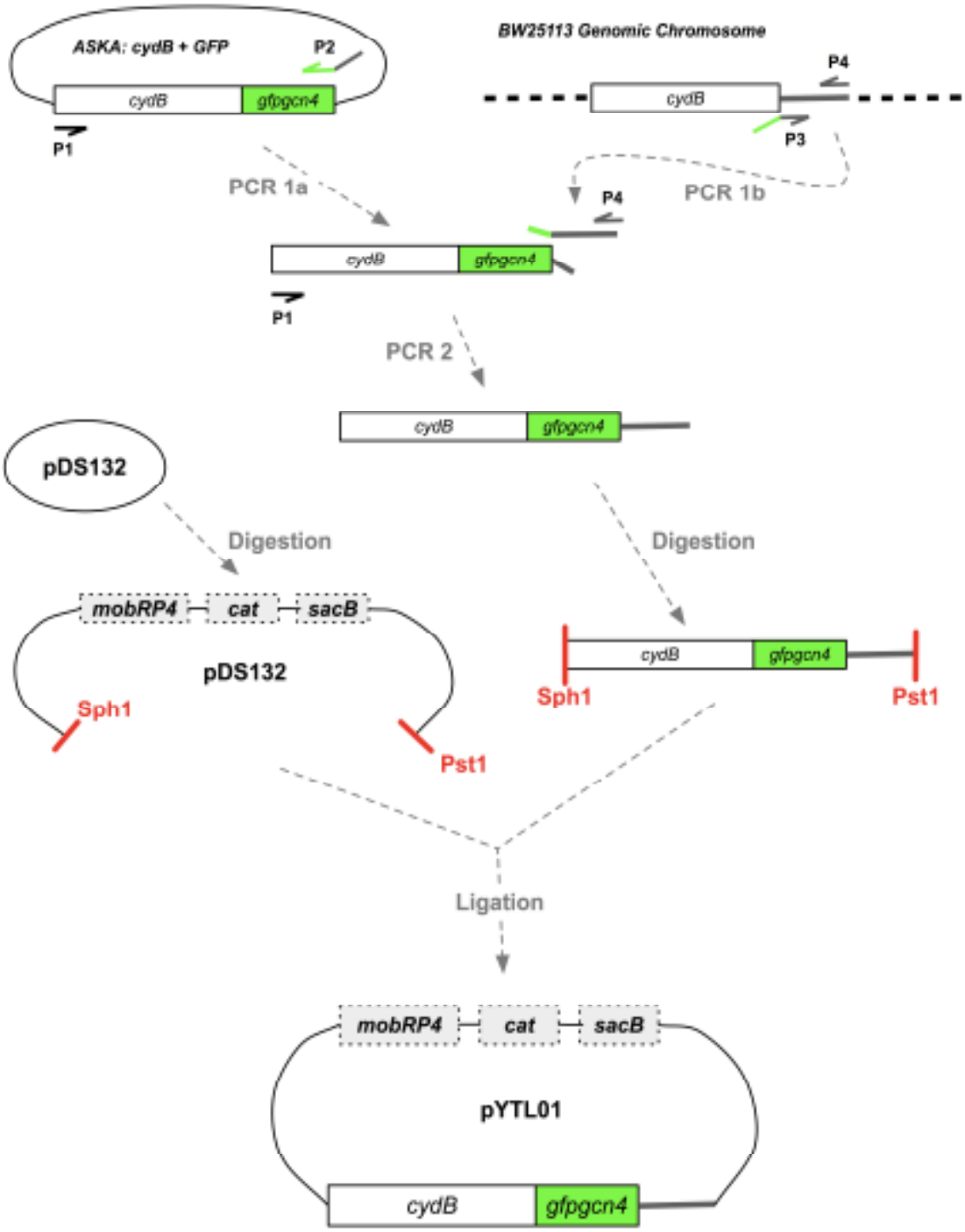

Supplementary figure 1:
Construction of pYTL01